Determination of Soil Sorptive Potential by Soil Water Isotherm

Shengmin Luo, A.M.ASCE[1]; Ning Lu, F.ASCE[2]; and Yi Dong, M.ASCE[3]

Abstract: Soil sorptive potential (SSP) has recently been conceptualized as the sum of four known electromagnetic potentials in soil: cation and surface hydration, van der Waals attraction, electrical attraction, and osmosis due to electrical double layer. The SSP is most pronounced near the soil particle or intracrystalline surface and rapidly decays with increasing distance therefrom, governing the highly spatially varying characteristics of many fundamental soil properties such as pore water pressure, soil water density (SWD), and soil water phase transition. A novel framework was developed to determine the functions of SSP and SWD, directly using the experimental soil water isotherm (SWI) data with the aid of closed-form SWI and SWD models. A wide spectrum of soil types was examined to validate the proposed framework. Results indicate that the SSP in these soils can vary up to six orders of magnitude within the first three layers of adsorbed water molecules, leading to abnormally high values in both water pressure ($\sim 10^3$ MPa) and SWD (1.26 g/cm^3) at the soil–water interface. The predicted SWD curves are comparable to the existing experimental SWD measurements, and the controlling parameters for the SSP calibrated by the predicted SSP curves also show good agreement with the values reported in the literature, all confirming the validity of the proposed framework. It is concluded that soil sorptive potential and soil water density functions can be reliably determined from soil water isotherm data. **DOI: 10.1061/(ASCE)GT.1943-5606.0002795.**

Author keywords: Soil sorptive potential (SSP); Soil water isotherm (SWI); Soil water retention curve; Total soil water potential; Soil matric potential; Adsorption; Capillarity.

Introduction

Adsorption has been long recognized as an essential physical mechanism of soil water retention (Edlefsen and Anderson 1943; Iwata 1972), but understanding and quantification of its connection with matric potential remains largely conceptual. To date, matric potential of soil water has been commonly defined, measured, and used as the pressure difference between pore water and pore air, which only accounts for the capillary mechanism (e.g., Lu 2020). The underlying assumption therein is that the pore water pressure can be treated as a constant averaged within a soil-water-air representative elementary volume (REV) typically greater than 1 μm in size. However, this widely used concept of matric potential only considers the capillary potential (also known as pressure potential) of soil water and cannot describe many fundamental physical phenomena occurring at scales less than the REV of matric potential, including variation of soil water density (SWD) (e.g., De Wit and Arens 1950; Martin 1962; Bahramian et al. 2017; Zhang and Lu 2018), supercooling in soil freezing temperature (e.g., Smith and Tice 1988; Watanabe and Wake 2009; Zhang and Lu 2021), and capillary cavitation and condensation (e.g., Bittelli and Flury 2009; Solone et al. 2012; Luo et al. 2021).

In soil, water exists in all pore scales: nanopore (<0.1 μm), micropore (5–30 μm), mesopore (30–75 μm), and macropore (>75 μm). Water in each of these pores is retained in distinct physical forms of adsorption and/or capillarity. Although the augmented Young-Laplace equation (Philip 1977; Nitao and Bear 1996) provides a more general definition of matric potential than the capillary potential by considering adsorption as a function of adsorbed water film thickness, it does not capture the highly spatially varying water properties due to adsorption. This inability is recently overcome by a breakthrough soil sorptive potential (SSP) theory (Lu and Zhang 2019). The SSP stems from four intermolecular forces that are all electromagnetic in origin. These forces highly depend on the spatial position in soil pores, imparting drastically decaying characteristics to the SSP with the increasing distance from the soil particle or intracrystalline surface.

The SSP theory states that matric potential represents the thermodynamic state of soil water and is always equal to the sum of SSP and capillary potential at any location inside the soil water body (Zhang and Lu 2019), following the principle of local thermodynamic equilibrium (Revil and Lu 2013; Lu 2016). Common experimental techniques for measuring the matric potential function or the soil water retention curve (SWRC) are tensiometer, axis translation, filter paper, and relative humidity. These methods together can cover a wide range of matric potential from about −400 to 0 MPa, but a much lower matric potential down to −2,000 MPa has been theorized or measured (e.g., Croney and Coleman 1961; Richards 1965; Campbell and Shiozawa 1992; Zhang et al. 2017). Since the early 2010s, dynamic dew point, or commercialized vapor sorption analyzer (VSA) (Likos et al. 2011; Lu 2020), has emerged as an efficient, reliable, and time-saving tool for measuring high-resolution soil water isotherm (SWI), typically

[1]Postdoctoral Fellow, Dept. of Civil and Environmental Engineering, Colorado School of Mines, Golden, CO 80401. ORCID: https://orcid.org/0000-0002-5433-6285. Email: shengminluo@mines.edu

[2]Professor, Dept. of Civil and Environmental Engineering, Colorado School of Mines, Golden, CO 80401 (corresponding author). ORCID: https://orcid.org/0000-0003-1753-129X. Email: ninglu@mines.edu

[3]Professor, State Key Laboratory of Geomechanics and Geotechnical Engineering, Institute of Rock and Soil Mechanics, Chinese Academy of Science, Wuhan, Hubei 430071, PR China. Email: ydong@wrsm.ac.cn

Note. This manuscript was submitted on June 11, 2021; approved on January 21, 2022; published online on March 23, 2022. Discussion period open until August 23, 2022; separate discussions must be submitted for individual papers. This paper is part of the ***Journal of Geotechnical and Geoenvironmental Engineering***, © ASCE, ISSN 1090-0241.

offering several hundreds of soil water retention (SWR) data points at the very low matric potential (−850 to −10 MPa) where adsorption dominates.

To determine a soil's sorptive potential from the measured SWRC, an iterative algorithm was recently developed (Zhang and Lu 2020), in which coupling between the SSP and SWD functions is needed. Because the SSP is identical to the adsorptive electromagnetic potentials at very low matric potential range where no capillary water would occur due to cavitation, a generalized SWR equation (Lu 2016) was first implemented to separate the adsorptive water from the capillary water. Only the former was then used to quantify the statistical distance from the soil particle surface at a given matric potential (Zhang and Lu 2020). However, typical SWR measurements in the adsorptive-dominated regime (< −10 MPa) are usually sparse, with less than 20 data points, and are uneven in measuring intervals (e.g., Likos and Lu 2003; Lu 2016; Dong and Lu 2020), not only limiting the accuracy of the SSP determination algorithm but also constraining the spatial extent of the SSP to no farther than the tightly adsorbed regime. In this work, a noniterative, uncoupled, yet more accurate and physically representative framework based on SWI measurements was developed to determine the SSP over the full range of relative humidity. The framework fully takes advantage of the recently developed analytical SWI equations that separate adsorptive and capillary water isotherms, and then the adsorptive water isotherm was used as the source of SSP while the capillary water isotherm was used as the boundary condition at the air–water interface. The proposed framework was experimentally validated by using the SWI data from different types of soils, including some end members of pure clay minerals.

Overview of Soil Sorptive Potential

The SSP $\psi_{\text{sorp}}(x)$ has been conceptualized and formulated as the sum of the four known electromagnetic potentials: cation and surface hydration $\psi_{\text{hyd}}(x)$, van der Waals $\psi_{\text{vdW}}(x)$, electrical attraction $\psi_{\text{ele}}(x)$, and osmosis $\psi_{\text{osm}}(x)$ (Zhang and Lu 2018; Lu and Zhang 2019)

$$\psi_{\text{sorp}}(x) = \psi_{\text{hyd}}(x) + \psi_{\text{vdW}}(x) + \psi_{\text{ele}}(x) + \psi_{\text{osm}}(x) \tag{1}$$

where x = minimum distance to the adjacent particle surface and represents the spatial coordinate (nm). The exchangeable cations are attracted to the clay surface and interlayer space during the formation of clay mineral to ensure the overall electric neutrality. When clayey soils are dry, water molecules are prone to first hydrate and concentrate around these exchangeable cations and the hydroxyl/oxygen exposed on the external surface of soil minerals. This is because such hydration process can provide the lowest (i.e., most negative) free energy change (< −12.5 kJ/mol) during the conversion from free water to soil water. The van der Waals force represents the attraction between soil solid and water molecule and is present in essentially all soil types, while the other three components are more pronounced in fine-grained soils, especially in clays. Clay particle surfaces are often negatively charged because of the isomorphous substitutions. This charged surface produces an electric field that imposes electric potential on the polar water molecules interacting with the soil matrix. Ions and exchangeable cations dissolved in soil water also redistribute and form the electrical double layer around the clay particles, consequently inducing local osmotic potential by the ion concentration gradient.

SSP governs soil's intrinsic properties such as the Hamaker constant, specific surface area (SSA), and cation exchange capacity (CEC). The magnitudes of four electromagnetic components of SSP decay nonlinearly as the distance to the particle surface increases (Lu and Zhang 2019; Zhang and Lu 2020). In general, SSP is dominated by van der Waals and hydration components within a short distance (up to several nanometers) to the soil particle surface, whereas the osmotic component caused by the electrical double layer can prevail over the other components at distances farther away (up to 1 μm). The degree of conversion between SSP and potential of adsorbate depends on the pore fluid properties (e.g., polarity, dielectric constant, and bulk concentration). For instance, water molecules with strong polarity will have all four SSP components in clays, but nonpolar nitrogen molecules only interact with clay particles via relatively weak nonpolar van der Waals forces.

Proposed Framework for Soil Sorptive Potential Determination

In soil, the SSP and matric potential are interconnected under the unitary definition of matric potential (Lu and Zhang 2019; Zhang and Lu 2019)

$$\psi_m(w) = \psi_{\text{sorp}}(x) + u_w(x, w) - u_a \tag{2}$$

where ψ_m and ψ_{sorp} = matric potential and SSP, respectively (MPa); u_w and u_a = pore water pressure and pore air pressure, respectively (MPa); and w = gravimetric water content (g/g) of soil equilibrated with the prevailing ambient conditions. Eq. (2) shows that matric potential is a sole function of soil water content (i.e., known as the SWRC), whereas SSP is a sole function of the distance x from the soil particle surface. This observation demonstrates the necessity of a scaling relationship between water content w and distance x for formulating a coupled conceptual and experimental framework to determine the SSP. The key ingredients of the proposed framework are described in the following together with the illustrations of fundamental SWR mechanisms.

Generalized SWI Model

SWI characterized by hygrometer-based approaches (e.g., VSA) describes the relationship between relative humidity (RH) and equilibrium water content in soil [Fig. 1(a)]. According to the Kelvin equation, total soil water potential ψ can be directly determined from a given RH (e.g., Lu and Likos 2004)

$$\psi = \frac{RT}{v_w}\ln(\text{RH}) \tag{3}$$

where R = universal gas constant (8.3145×10^{-3} kJ·mol^{-1}·K^{-1}); T = temperature (K); and v_w = molar volume of water (1.8×10^{-5} m^3/mol at 0.1013 MPa and 25°C). The total potential ψ and matric potential ψ_m can be considered equivalent when gravitational and bulk osmotic potentials are negligible in magnitude. Thus, the experimental isotherm data [Fig. 1(a)] commonly measured at RH range of 0.03–0.95 represent the SWRC at relatively low matric potential [Fig. 1(b)]. Because the SWI measured by VSA or other similar techniques generally records abundant data points, it provides a promising way to accurately quantify the adsorptive characteristics of a soil.

Adsorption, capillarity, and cavitation or capillary condensation are three major physical mechanisms dictating the SWR process (e.g., Revil and Lu 2013; Lu 2016). A SWI model recently proposed by Luo and Lu (2021) showed the robustness of fitting the experimental SWI data at the full range of RH from nearly 0 to 1. This is achieved by expressing the total soil water content w under an equilibrium RH as a mathematical sum of adsorptive and capillary components

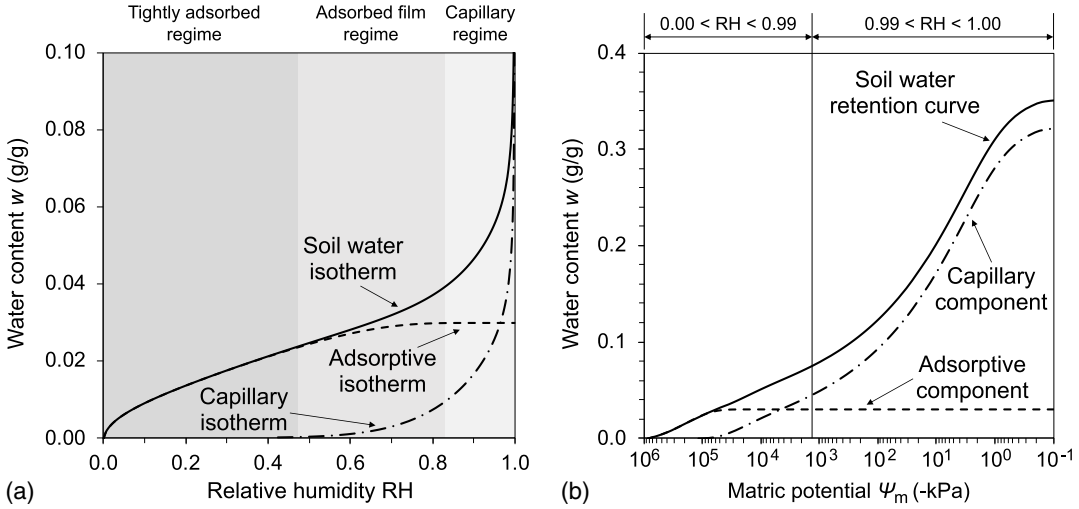

Fig. 1. Three soil water retention regimes at different ranges of relative humidity and matric potential in terms of (a) relative humidity; and (b) matric potential.

$$w(\mathrm{RH}) = w_{\mathrm{ad}}(\mathrm{RH}) + w_{\mathrm{cap}}(\mathrm{RH}) \tag{4}$$

$$w_{\mathrm{ad}}(\mathrm{RH}) = w_{\mathrm{amax}}\left\{1 - \left[\exp\left(1 - \frac{\ln(\mathrm{RH_{min}})}{\ln(\mathrm{RH})}\right)\right]^{1-1/n}\right\} \tag{5}$$

$$w_{\mathrm{cap}}(\mathrm{RH}) = \left[\Phi\left(\frac{\mathrm{RH}-\xi}{\omega}\right) - 2\mathrm{T}\left(\frac{\mathrm{RH}-\xi}{\omega}, -5\right)\right] \times [w_s - w_{\mathrm{ad}}(\mathrm{RH})] \times \left\{1 + \left[-\frac{RT\ln(\mathrm{RH})}{v_w}\right]^n\right\}^{1/n-1} \tag{6}$$

where w_{ad} and w_{cap} = adsorptive and capillary water contents, respectively; w_{amax} = gravimetric adsorption capacity (g/g); w_s = saturated gravimetric water content determined by the specific gravity and porosity (g/g); $\mathrm{RH_{min}}$ = minimum relative humidity corresponding to a completely dry condition; and n = parameter related to soil's pore size distribution. The effects of cavitation/capillary condensation on SWI are cast in Eq. (6) by using a cumulative distribution function (CDF) of a skew-normal distribution. This cavitation function includes two parts, i.e., the CDF of a normal distribution $\Phi()$ and Owen's T function $\mathrm{T}()$, and is defined by three cavitation parameters, i.e., onset relative humidity ξ, cavitation humidity range ω, and CDF shape parameter α. The last parameter α can be substituted by a constant of -5 for most soils (Luo and Lu 2021).

Fig. 1(a) illustrates how the SWI is divided into the adsorptive isotherm and the capillary isotherm, which helps identify three distinct regimes of the soil water retention process, namely, the tightly adsorbed, adsorbed film, and capillary regimes. In the tightly adsorbed regime, water molecules are strongly bonded to the soil particle surfaces by the aforementioned four electromagnetic forces of SSP, such that the adsorptive water can be interpreted as a water film with uniform thickness coating on the soil particle surfaces [Fig. 2(a)]. As the water film becomes thicker with increasing water content, SSP also increases (i.e., becomes less negative) drastically, and water molecules in the outside layer are bonded by relatively weak van der Waals forces. Meanwhile, water vapor starts to condense in capillary form at the corners of soil particles by connecting the adjacent water films. This transition process (i.e., the adsorbed film regime) will last until multilayer adsorption is complete, after which SSP diminishes and capillarity dominates the soil–water interactions. The maximum amount of water that can be retained by a soil in the form of adsorption is captured in Eq. (5) by the adsorption capacity w_{amax}.

Determination of SSP through Matric Potential at Air–Water Interface

The SSP, as an intrinsic property of soil, can convert into both matric potential and water pressure (Zhang and Lu 2020); thus, the pore water pressure term u_w in Eq. (2) can be further split into the adsorptive pressure $u_{w\text{-ad}}$ and the capillary pressure $u_{w\text{-cap}}$ components (Lu 2020)

$$\psi_m(w) = [\psi_{\mathrm{sorp}}(x) + u_{w-\mathrm{ad}}(x,w)] + [u_{w-\mathrm{cap}}(w) - u_a] \tag{7}$$

According to Eq. (4), adsorption and capillarity coexist under the same RH (i.e., matric potential) at thermodynamic equilibrium, although they are two different mechanisms of soil–water interactions with distinct free energy levels. By analogy with the ideal gas law, Eq. (4) further implies that the relative amount of different water contents reflects the distribution of soil water energy (i.e., the water potential) stored in different forms, which provides the rationale to distinguish the free energy contributions of adsorption and capillarity to matric potential, i.e.

$$\psi_m(w) = \psi_m(w)\frac{w_{\mathrm{ad}}(\psi_m) + w_{\mathrm{cap}}(\psi_m)}{w(\psi_m)} = \psi_m(w)\left[\frac{w_{\mathrm{ad}}(\psi_m)}{w(\psi_m)} + \frac{w_{\mathrm{cap}}(\psi_m)}{w(\psi_m)}\right] \tag{8}$$

Comparing Eq. (8) with Eq. (7) leads to

$$\psi_{\mathrm{sorp}}(x) + u_{w-\mathrm{ad}}(x,w) = \psi_m(w)\frac{w_{\mathrm{ad}}(\psi_m)}{w(\psi_m)} \tag{9a}$$

$$u_{w-\mathrm{cap}}(w) - u_a = \psi_m(w)\frac{w_{\mathrm{cap}}(\psi_m)}{w(\psi_m)} \tag{9b}$$

The deduction here implicitly considers a homogenized soil water body for simplicity, even though in reality there is a

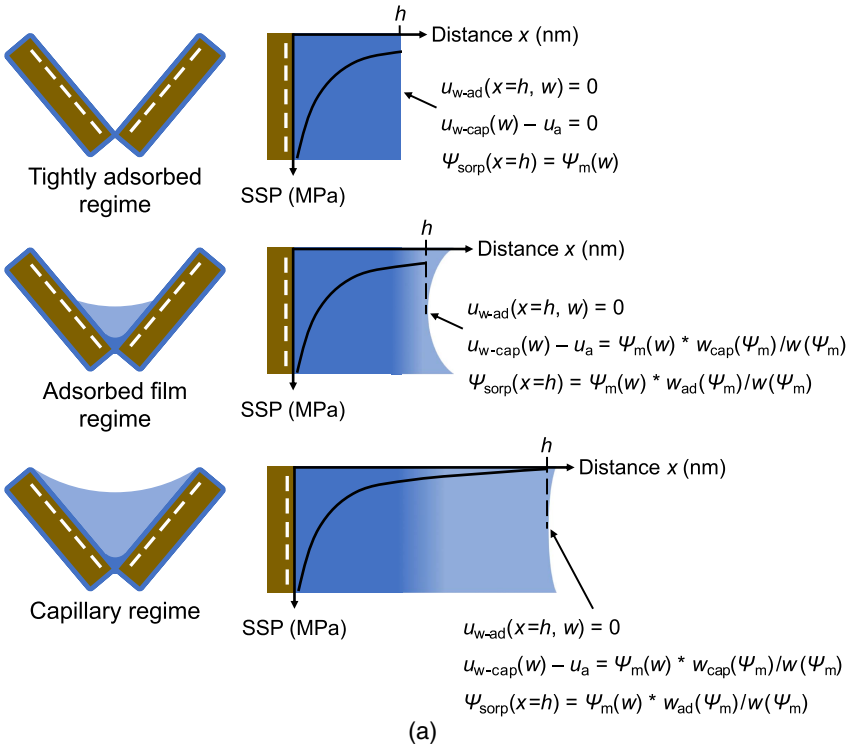

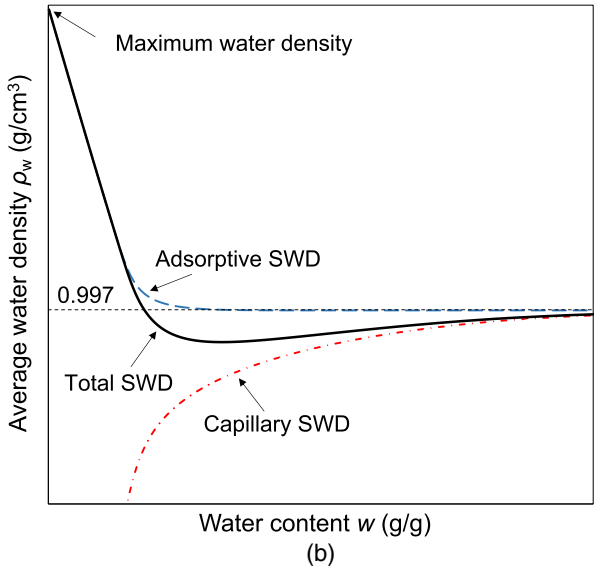

Fig. 2. (a) Determination of soil sorptive potential based on the fitted soil water isotherm/soil water retention curve; and (b) soil water density curve.

spatial differentiation between adsorptive water and capillary water.

The preceding generalized formulas for matric potential will be simplified into different expressions for different SWR processes. For instance, at the tightly adsorbed regime where no capillary water content is identified by the SWI model (i.e., $w_{cap} = 0$), only adsorption occurs and the air–water interface is flat, as illustrated in Fig. 2(a). In this case, the capillary potential is zero, indicating the equivalence of interfacial pressure between the air phase and the water phase

$$u_{w-\text{cap}}(w) - u_a = 0 \tag{10}$$

Because the intermolecular water pressure at the air–water interface is determined by the force equilibrium among water molecules along the interface (i.e., capillarity), a boundary condition of $u_{w-\text{ad}}(x = h, w) = 0$ can be imposed for the adsorptive water pressure. Then Eq. (7) is rewritten as

$$\psi_{\text{sorp}}[x = h(w)] = \psi_m(w) \tag{11}$$

and the SSP at the air–water interface is numerically equivalent to matric potential.

Therefore, the magnitude of capillary potential depends on the prevailing ambient condition [Eq. (9*b*)]. Once the SWR process is in transition from adsorptive to capillary regimes, a curved air–water interface starts to appear in small pores [Fig. 2(a)], generating a pressure deficit in the liquid phase. With the aid of the SWI model and Kelvin equation, the magnitude of adsorptive component of matric potential (i.e., the SSP) at the air–water interface can be

determined from the SWI data for a specific water content (SSP versus w)

$$\psi_{\text{sorp}}[x = h(w)] = \psi_m(w)\frac{w_{\text{ad}}(\psi_m)}{w(\psi_m)} \tag{12}$$

Again, the preceding equation is a general expression that can be reduced to Eq. (11) when the SWR only involves adsorption (i.e., $w = w_{\text{ad}}$).

Scaling from Soil Water Content to Local Distance

To characterize how the SSP varies with the statistical distance x via the function of SSP versus soil water content w, a simple scaling relationship as follows can be used (Tuller and Or 2005; Zhang and Lu 2020):

$$w = x \times \text{SSA} \times \rho_w(w) \tag{13}$$

where SSA = specific surface area of a soil (m^2/g); and ρ_w = average SWD (g/cm^3) at the water content w.

The dimension of the water molecule is not considered in the preceding equation such that the water film can be treated as a continuum to maintain the pore water pressure concept [i.e., the validity of Eq. (2)] even at very low water content. In addition, this scaling relationship originally proposed for the tightly adsorbed water film is also assumed to be generally applicable to the adsorption-capillarity transition process, which can be physically justified as follows. As illustrated in Fig. 1(a), SSP is still the dominant mechanism in the transition (i.e., adsorbed film) regime if considering the much higher adsorptive water content than the capillary water content. The second soil-water-air REV shown in Fig. 2(a) also demonstrates that water molecules at the air–water interface are subjected to the effects of both adsorption and capillarity that may not be completely and physically separable. For most soils, capillary water content will only be comparable to adsorptive water content when RH is greater than ~0.9, corresponding to matric potential $\psi_m > -14.5$ MPa. Tuller and Or (2005) suggested that capillary condensation will only play a role in SWR for high enough matric potential (> -10 MPa), whereas the magnitude of SSP in this range is no longer significant compared with that found near the soil particle surface. Therefore, the error introduced by approximating the statistical distance x with the scaling Eq. (13) is trivial beyond the tightly adsorbed regime.

It has been found that adsorption and capillarity oppositely affect the water density in soil (Zhang and Lu 2018). The attractive forces of SSP always result in a positive, locally varying, water pressure that compacts the water molecules toward a higher density. On the contrary, capillarity homogeneously develops intermolecular tension among all water molecules, lowering the water pressure below the ambient air pressure and hence reducing the water density. Clearly, for a given water content, the interplay of adsorptive and capillary effects determines the water density averaged over the soil water body, so the SWD curve will be highly related to the SWRC.

In this study, the adsorptive part of SWD $\rho_{w\text{-ad}}$ is described by an exponentially decaying function

$$\rho_{w-\text{ad}}(w) = (\rho_{\max} - \rho_0)\exp\left[\eta - \frac{\eta\psi_{\min}}{\psi_m(w)}\right] + \rho_0 \tag{14}$$

where ρ_0 = free water density ($0.997\ \text{g}/\text{cm}^3$); $\rho_{\max}$ = maximum soil water density (g/cm^3); $\psi_{\min}$ = lowest matric potential (MPa) corresponding to the $\text{RH}_{\min}$ presented in Eq. (5); and η = decay rate. The capillary part of SWD $\rho_{w\text{-cap}}$ can be calculated as

$$\rho_{w-\text{cap}}(w) = \rho_0 \exp[k_0\psi_m(w)] \tag{15}$$

where k_0 = isothermal compressibility of water ($4.6 \times 10^{-4}\ \text{MPa}^{-1}$ at 25°C). As schematically illustrated in Fig. 2(b), the total SWD is a weighted average obtained from its two constituent parts in terms of individual water content fractions

$$\rho_w(w) = \rho_{w-\text{ad}}(w)\frac{w_{\text{ad}}(\psi_m)}{w(\psi_m)} + \rho_{w-\text{cap}}(w)\frac{w_{\text{cap}}(\psi_m)}{w(\psi_m)} \tag{16}$$

Two parameters in Eq. (14), i.e., $\rho_{\max}$ and η, need to be determined from the experimental SWI data. The maximum water density is the result of the extremely high intermolecular water pressure, which usually associates with the first-layer hydration occurring around the exchangeable cations and the clay particle surfaces. Herein, the highest water pressure occurs on the soil particle surface when matric potential is the lowest (Zhang and Lu 2020). Focusing on the pressure-induced dense-packing effect and ignoring the structural change of water molecules, the maximum water density $\rho_{\max}$ can be calculated by the Tait equation (e.g., Hayward 1967)

$$\rho_{\max} = \rho_0 \Bigg/ \left[1 - \frac{-\psi_{\min} - u_a}{k_0^{-1} + m_v(-\psi_{\min} - u_a) + n_v(-\psi_{\min} - u_a)^2}\right] \tag{17}$$

where m_v and n_v = two constants experimentally calibrated as 3.32 (unitless) and -4.54×10^{-4} (MPa^{-1}), respectively (Cho et al. 2002). A proper value for the decay rate η will be determined subsequently.

SSP Determination Procedure

As shown in the preceding subsections, SSP, SWRC, SWD, and SSA are fundamentally interconnected under the unitary definition of matric potential Eq. (2). In particular, SSP and SWD functions can be regarded as twin soil characteristic curves, given that SSP is the physical source of SWD, while in turn SSP is determined on the basis of SWD. Because SSP and the adsorptive part of matric potential are equivalent at the air–water interface, the former can be experimentally quantified for a given soil if SWRC is converted from SWI.

The procedure for SSP determination from SWI data is summarized in Fig. 3 and elaborated as follows. First, the generalized SWI model [Eqs. (4)–(6)] is used to fit the experimental SWI data such that the measured isotherm data can be separated into the adsorptive isotherm and capillary isotherm over the full range of relative humidity. Second, a sufficient number of RH values are sampled with appropriate intervals for both the fitting visualization and further data processing. In this study, a total of 300 RH points were used to ensure the subsequently determined SSP function is smooth and continuous. These manually selected data points included 100 isometric samplings for each of the three RH ranges: $\text{RH}_{\min}$–0.5, 0.51–0.99, and 0.991–0.99999. The three fitted isotherm curves, i.e., total SWI, adsorptive isotherm, and capillary isotherm [e.g., Fig. 1(a)], are calculated at the selected RH locations using the model parameters. The corresponding SWRCs to the isotherms are obtained through the Kelvin equation [Eq. (3)], as shown in Fig. 1(b). Once the SWD function is determined by using Eqs. (14)–(17), the SSP curve of a soil can be calculated in the last step by incorporating the SWD function into Eqs. (12)–(13).

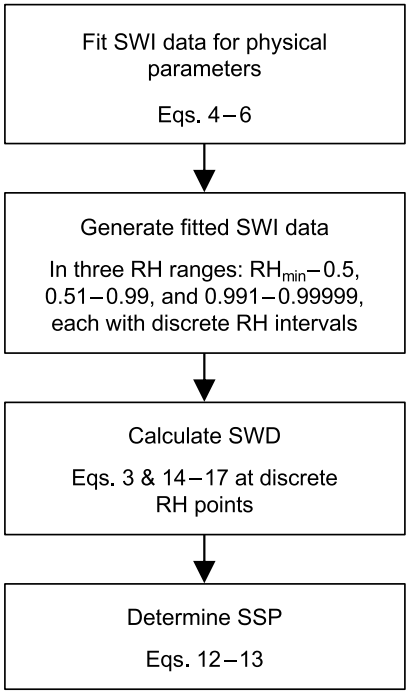

Fig. 3. Flowchart for determining the SSP function from soil water isotherm.

Experimental Validation

SWI Data Set and SWI Model Fitting

Experimental SWI data measured for eight different soils were used to determine their SSP functions and to verify the proposed framework. Table 1 summarizes some basic soil physical and geotechnical index properties for soil classification. The selected soils were deemed representative of a variety of soil types from sandy silt (e.g., Balt silt II) to swelling clays (e.g., Wyoming montmorillonite and Denver bentonite), covering plasticity index (PI) from 5 to 185, SSA from 26 to 594 m^2/g, and CEC from 9 to 169 cmol/kg. These soils were equally divided into two groups based on their testing approaches for the vapor sorption experiment. The SWI data in the first group were from the current study conducted with a dynamic water vapor sorption (ProUmid GmbH, Ulm, Germany), while data in the second group were obtained with a vapor sorption analyzer (Meter Group, Pullman, Washington) from the literature, i.e., Balt silt II from Khorshidi and Lu (2017) and the others from Zhou and Lu (2021). A complete sorption experiment generally includes an adsorption-desorption cycle, mostly covering the RH range from about 0.03 to 0.95 with about 200 measured data points. Details of the SWI testing procedure for VSA can be found in Likos et al. (2011). The major difference between the two groups of SWI data is that a much lower RH limit of 0.002 (i.e., a wider RH range) can be attained in the first group through the dynamic water vapor sorption equipment.

The best-fit SWI parameters [Eqs. (4)–(6)] to the data on the wetting path are listed in Table 2, where constant values are also assumed for specific gravity G_s (i.e., 2.65) and porosity ϕ (i.e., 0.5) if the actual measurements from tested samples are not available. The goodness of fit for soils in both groups can be visually assessed in Figs. 4 and 5. Overall, the SWI model can be used to accurately represent isotherms of all types of soil. The best-fit isotherm curve for each soil nearly perfectly follows the experimental data points over the entire range of RH, consequently providing a very high coefficient of determination R^2 equal to 1.00. The adsorptive and capillary water contents are explicitly separated under the same RH (i.e., the same matric potential) using Eqs. (5)–(6). The fitted adsorption capacity w_{amax} (Table 2) increases as the soil becomes finer from silty soil (e.g., 0.005 g/g for Georgia kaolinite and 0.024 g/g for Balt silt II) to bentonite clays (e.g., 0.14 g/g for Denver bentonite and 0.20 g/g for Wyoming montmorillonite), quantitatively confirming the ability of the SWI model to characterize the adsorption behaviors of different soil types.

Calculated SWD Curves

All the necessary parameters for calculating the SWD curve [Eqs. (14)–(17)], except for the decay rate η, will be available once the fitted SWRCs are identified from the fitted isotherms (e.g., Fig. 1). The parameter η controls how drastic the average SWD curve exponentially decreases with the increasing water content. For instance, a lower η value will lead to a more gradual change of SWD, and vice versa (Zhang and Lu 2018). Because kaolinite and sodium montmorillonite are well known as the two end members that respectively represent both low- and very high-plasticity soils, a representative value of η can be obtained from a parametric study conducted for soils in Group 1. Fig. 6 exhibits the experimentally measured SWD data of different clays reported in the literature (De Wit and Arens 1950; Bahramian et al. 2017; Zhang and Lu 2018; Dong et al. 2020), in which Ningming clay is a swelling clay with an SSA of 375 m^2/g comparable to

Table 1. Physical and geotechnical index properties of the eight studied soils

Group	Soil name	LL (%)[a]	PL (%)[a]	PI	USCS	Total SSA (m^2/g)[a]	CEC (cmol/kg)	Swelling potential[b]
1	Georgia kaolinite	44	26	18	CL	26	9.0[c]	High
	Denver claystone	44	23	21	CL	67	35.0[c]	High
	Wyoming montmorillonite	218	33	185	CH	594	75.0[c]	Very high
	Denver bentonite	118	45	73	CH	591	169.0[c]	Very high
2	Balt silt II[c]	28	23	5	SM	47	24.0[c]	Low
	Wuhan clay[a]	40	18	22	CL	94	15.4[a]	High
	Xinyang clay[a]	42	19	23	CL	114	20.6[a]	High
	Jingmen yellowish-brown soil[a]	63	26	37	CH	251	30.9[a]	Very high

Note: PI = plasticity index; LL = liquid limit; PL = plastic limit; and USCS = Unified Soil Classification System.
[a]Zhou and Lu (2021).
[b]Chen (1988).
[c]Khorshidi and Lu (2017).

Table 2. Results of the fitted parameters for the SWI model

Group	RH range of data	Soil name	Specific gravity, G_s	Porosity, ϕ	Minimum RH, RH_{min}	Adsorption capacity, w_{amax} (g/g)	PSD parameter, n	Onset RH, ξ	Cavitation RH range, ω	Coefficient of determination, R^2
1	0.002–0.950	Georgia kaolinite	2.65	0.57	0.0022	0.005	1.39	1.00	0.24	1.00
		Denver claystone	2.65	0.50	0.0023	0.030	1.29	0.96	0.20	1.00
		Wyoming montmorillonite	2.65	0.70	0.0022	0.200	1.07	1.00	0.03	1.00
		Denver bentonite	2.65	0.70	0.0008	0.140	1.30	0.93	0.15	1.00
2	0.03–0.95	Balt silt II	2.65	0.50	0.0049	0.024	1.30	1.00	0.22	1.00
		Wuhan clay	2.73	0.50	0.0047	0.032	1.20	1.00	0.16	1.00
		Xinyang clay	2.72	0.50	0.0004	0.046	1.20	1.00	0.21	1.00
		Jingmen yellowish-brown soil	2.75	0.50	0.0003	0.075	1.14	1.00	0.15	1.00

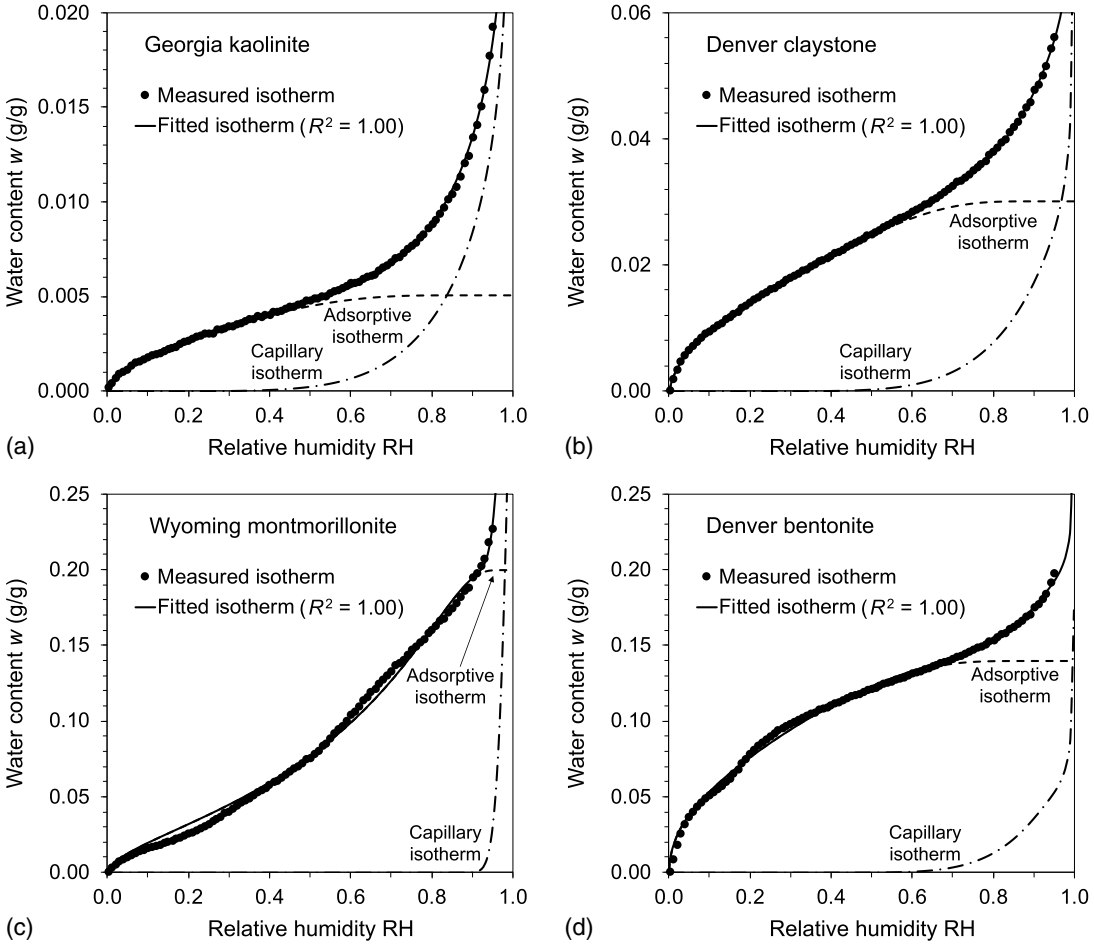

Fig. 4. Fitted soil water isotherms and separated adsorptive and capillary isotherms for four different soils in Group 1.

bentonite soils. Four SWD curves calculated using $\eta = 0.2$ are also presented in Fig. 6. Direct comparisons between experimental data and empirical model calculations manifest that the SWD curves predicted for Georgia kaolinite and Denver bentonite can enclose most of the physical measurements for a wide range of water content variation (e.g., 0.00–0.25 g/g). As such, 0.2 is good enough to serve as a reference value of η and is applied to determine the SWD curves of all soils. Additionally, the higher SWD measurement of Na-montmorillonite than the prediction observed at the dry end (Fig. 6) is likely attributed to the structural change of water molecules (Zhang and Lu 2018), which is not considered in the current SWD model.

In Fig. 6, the highest SWD values are obtained at the water content near zero, varying from 1.22 to 1.24 g/cm^3 for the four soils in Group 1. Despite the consistent observation of a nonlinearly decaying feature, effects of capillarity on the SWD curves fundamentally depend on the soil's adsorptive properties. For instance, Georgia kaolinite shows a sharp dip in SWD below the free water density at the water content of 0.01 g/g, indicating the dominance of capillary tension when the adsorptive ability of a soil is relatively

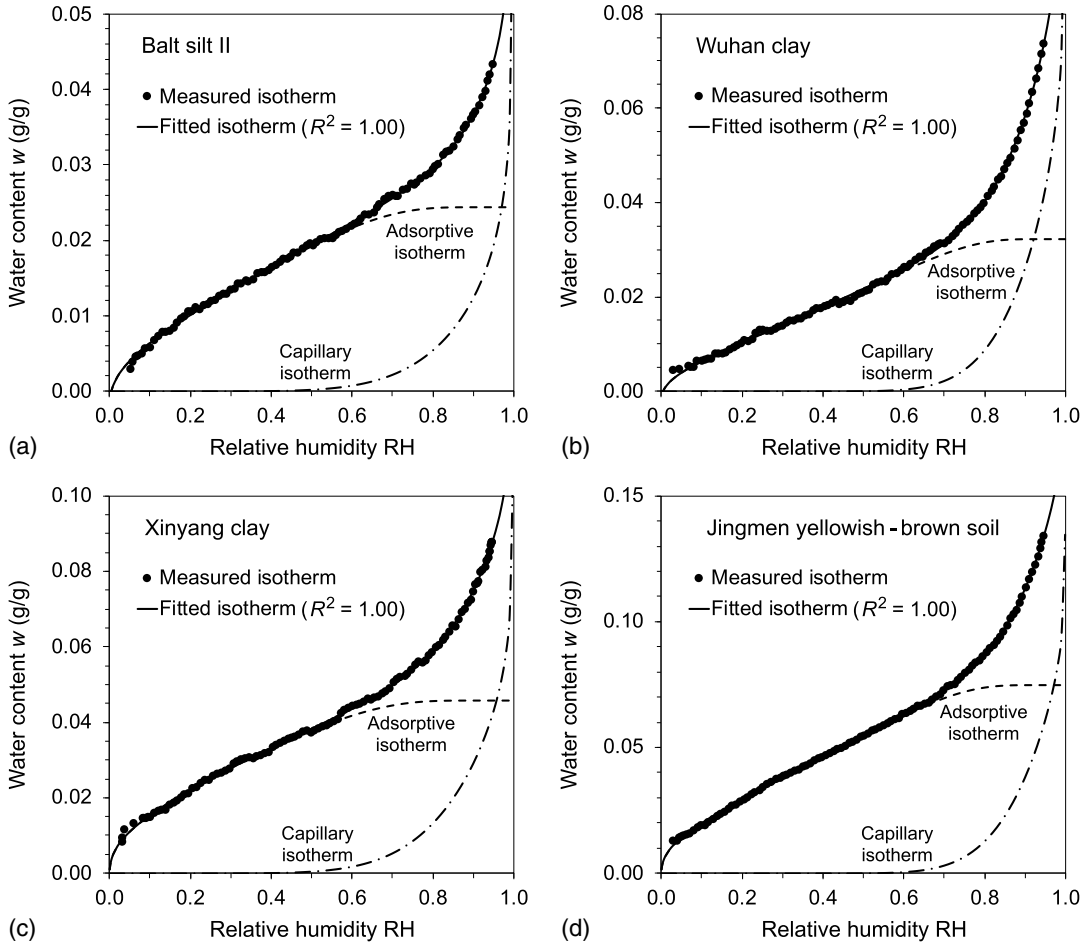

Fig. 5. Fitted soil water isotherms and separated adsorptive and capillary isotherms for four natural soils in Group 2.

weak. Such phenomenon is insignificant for the other three clays because their adsorption capacities w_{amax} are identified to be much higher than that of kaolinite (Table 2). Therefore, adsorption is an important physical mechanism that directly determines the abnormally high water density near the soil–water interface. Explicit consideration of the spatially varying SSP in the definition of matric potential is necessary for a better description of the fundamental soil properties such as SWD.

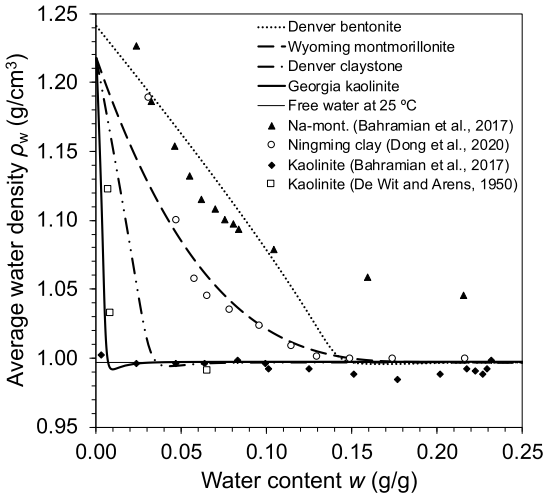

Fig. 6. Comparisons of experimental SWD data and SWD curves predicted by using the exponential decay rate $\eta = 0.2$.

Calculated SSP Curves

The SSP curves of four Group 1 soils obtained by using the proposed framework are plotted in Fig. 7. For each soil, the SSP decays drastically as the water content increases from oven-dryness [Fig. 7(a)]. To further explore the relationship between SSP and the distance x to the particle surface, Fig. 7(b) was generated by combining Figs. 6 and 7(a) via the scaling law Eq. (13). At a location near the particle surface, the highest (i.e., least negative) SSP value of −837 MPa and the lowest (i.e., most negative) SSP value of −983 MPa were identified from Denver claystone and Denver bentonite, respectively. Regardless of the soil type, the SSP curve almost always diminishes to a negligible magnitude (e.g., >-1 MPa) at a distance of 0.8 nm, which is equivalent to about three layers of adsorbed water molecules (~0.28 nm in diameter). The reason is that soils with a larger SSA (e.g., Wyoming montmorillonite) can retain a higher adsorptive water content than soils with a lower SSA (e.g., Georgia kaolinite), according to the scaling Eq. (13).

Unlike nonexpansive clays of Georgia kaolinite and Denver claystone whose SSP curves exponentially vary over six orders of magnitude, Figs. 7(c and d) further illustrate that the decrease in SSP curves for expansive clays of Wyoming montmorillonite and Denver bentonite is also accompanied by a sudden change in slope as the statistical distance x increases. Such phenomenon can be

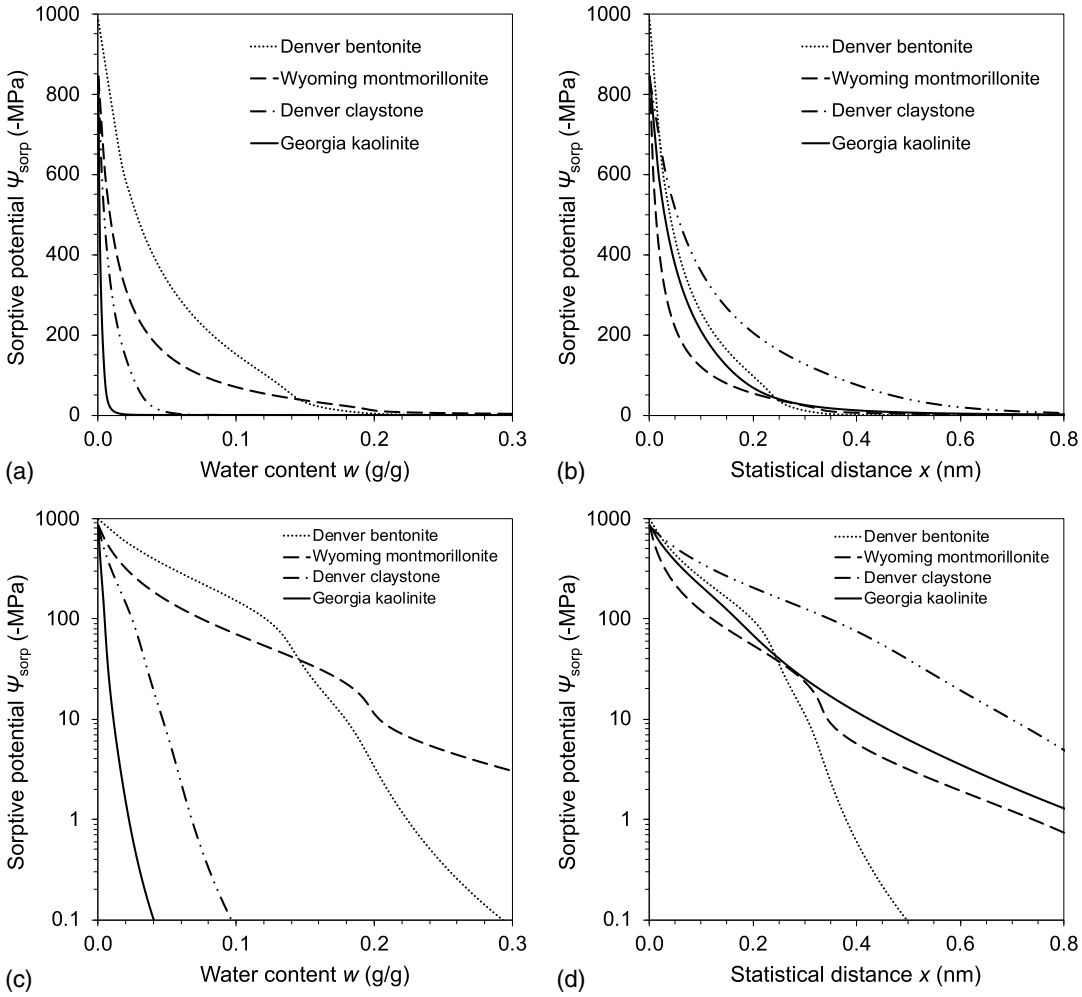

Fig. 7. (a and c) Predicted SSP as a function of water content for four different clays in terms of both linear scale and semi-log scale; and (b and d) scaled SSP curves from water content to statistical distance.

attributed to the initiation of capillary condensation, based on Fig. 7(c) and the isotherms of these two soils [Figs. 4(c and d)]. For soils with very fine particle size and strong adsorptive ability, the transition regime, i.e., the RH range between emergence of capillary water content and completion of adsorptive water content, is drastic or even nonexistent. In this case, capillary water can only exist in relatively large pores because water molecules adsorbed in small pores are completely dominated by the SSP and film water persists (Luo et al. 2021).

A similar observation of sharp decrease in SSP was also documented by Zhang and Lu (2020), in which the transition from adsorptive- to capillary-dominated mechanisms was assumed to be complete instantaneously due to the lack of high-resolution data of SWRC at low matric potential. However, results from the current study show that the transition process may be significant for some soils and can span a wide range of matric potential [e.g., Figs. 4(a and b)]. The proposed framework enables a better characterization of SSP in this regime so as to capture the distinct behaviors of SSP for different soils.

Georgia kaolinite and Wyoming montmorillonite are well-studied soils for their mineralogy and fundamental properties, such that they were used here to further validate the proposed framework for SSP determination. Comparisons were drawn between the SSP curves experimentally determined from the proposed framework and those theoretically calculated from the SSP theory (Lu and Zhang 2019) with the independent fundamental properties reported in the literature (Novich and Ring 1984; Lu et al. 2008; Lu and Zhang 2019). Beginning from the dry state, the sequence of soil water retention starts with the cation/surface hydration and van der Waals attraction, which dominate the SSP within the first few layers of water adsorption for their lowest free energy levels. Thus, the controlling parameters of cation hydration and van der Waals components, i.e., decay length of structural parameter λ_c and Hamaker constant A_H, can be calibrated for the two pure clay minerals by using the experimentally derived SSP curves. For simplicity, constant values were assigned to the controlling parameters of other nondominant SSP components. Specifically, a constant bulk ion concentration of 0.001 mol/m^3 was assumed for both clays. Additionally, −0.32 MPa and 0.2 nm were used for the surface hydration component and its pertinent decay length. Values of −3.50 and −6.03 mC/m^3 were applied to surface charge density of Georgia kaolinite and Wyoming montmorillonite, respectively (Guo and Yu 2017). Other physical parameters such as SSA and CEC can be found in Table 1. In addition, a minimum distance of 0.14 nm (i.e., dimension of half a water molecule) was imposed in the theoretical SSP model to avoid unrealistically low SSP values.

The experimentally determined and theoretically calculated SSP profiles of each clay are directly compared in Fig. 8, from which a good match can be observed in terms of a coefficient of

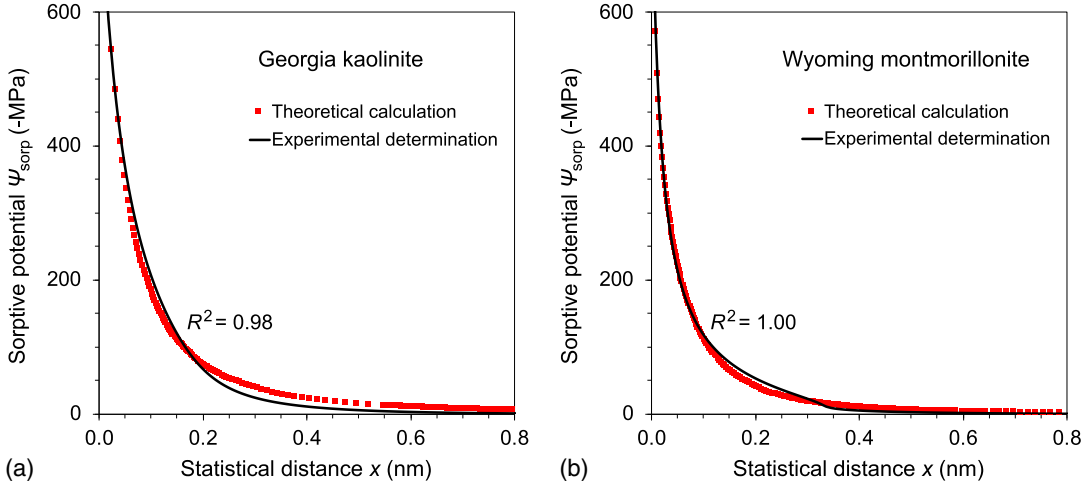

Fig. 8. Comparisons between the experimentally determined soil sorptive potential curve and theoretical calculation for two end-member clay minerals: (a) Georgia kaolinite; and (b) Na-montmorillonite.

determination $R^2 \geq 0.98$. The fitted Hamaker constants A_H are 3.3×10^{-20} J for Georgia kaolinite and 2.3×10^{-20} J for Wyoming montmorillonite, showing close agreement with the values reported in the literature (e.g., Novich and Ring 1984; Lu et al. 2008). The fitted decay lengths of structural parameter λ_c are 0.5 nm for kaolinite and 0.2 nm for montmorillonite, which also fall inside the reasonable range of 0.1–1.0 nm (Lu and Zhang 2019). For each clay, the subtle difference in two SSP profiles can be potentially caused by the simplifications performed on the osmotic and electrical components. Despite that, the validity of the proposed framework has been examined with quantitative evidence, confirming the capability of the framework to determine the SSP in different soil types.

Calculated Pore Water Pressure Curves

A uniform pore water pressure defined at the scale of matric potential REV has been commonly used to analyze virtually all geotechnical engineering problems. However, the SSP in soil provides the physical source that generates spatial variation of water pressure within the soil's REV [Eq. (2)], leading to inadequacy of the commonly used pore water pressure concept for solving many problems such as abnormally high soil water density and water phase transition. Four natural soils from Group 2 were examined to illustrate different characteristics of pore water pressure profile among a wide range of soil types (Table 2).

Fig. 9(a) shows the calculated SWD curves using parameter $\eta = 0.2$. The maximum soil water density varies from 1.26 g/cm^3 for the highly swelling Jingmen yellowish-brown soil to 1.20 g/cm^3 for the nonswelling Balt silt II. Regardless of the soil type, all SWD curves approach the free water density (0.997 g/cm^3) exponentially as the water content increases. Although this exponentially decaying SWD curve can lead to a slightly nonlinear variation in the initial portion of scaling Eq. (13), an overall linear function can still be used to describe the relationship between soil water content w and local distance x [Fig. 9(b)]. In addition, Fig. 9(b) also demonstrates that the scaled distance x depends more on the soil's SSA than SWD. For example, Jingmen yellowish-brown soil, i.e., a clayey soil with an SSA of 251 m^2/g, can retain over five times more water than that of the Balt silt II, i.e., a silty soil with an SSA of 47 m^2/g, at the monolayer coverage ($x = 0.14$ nm).

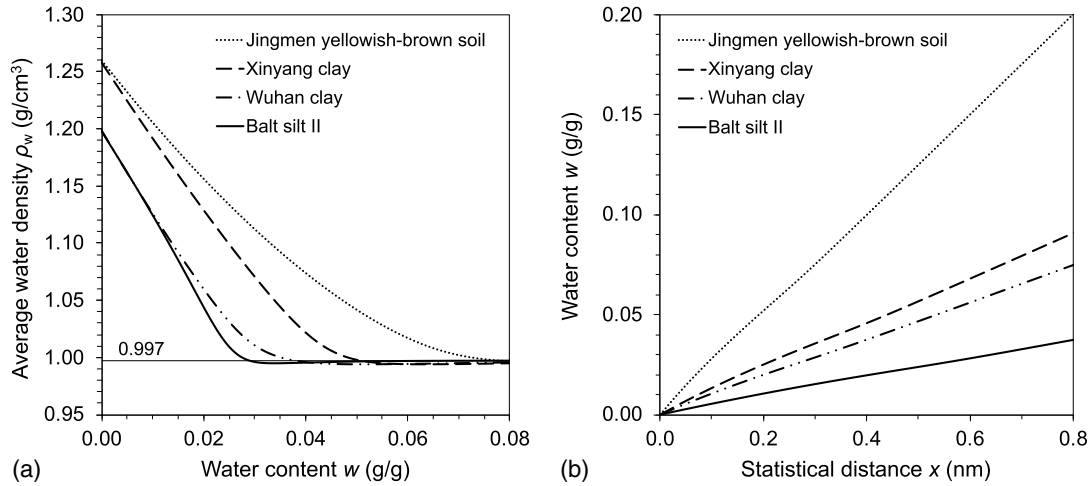

Fig. 9. (a) Distributions of soil water density functions for four natural soils; and (b) corresponding scaling relationship between water content and statistical distance from the soil particle surface.

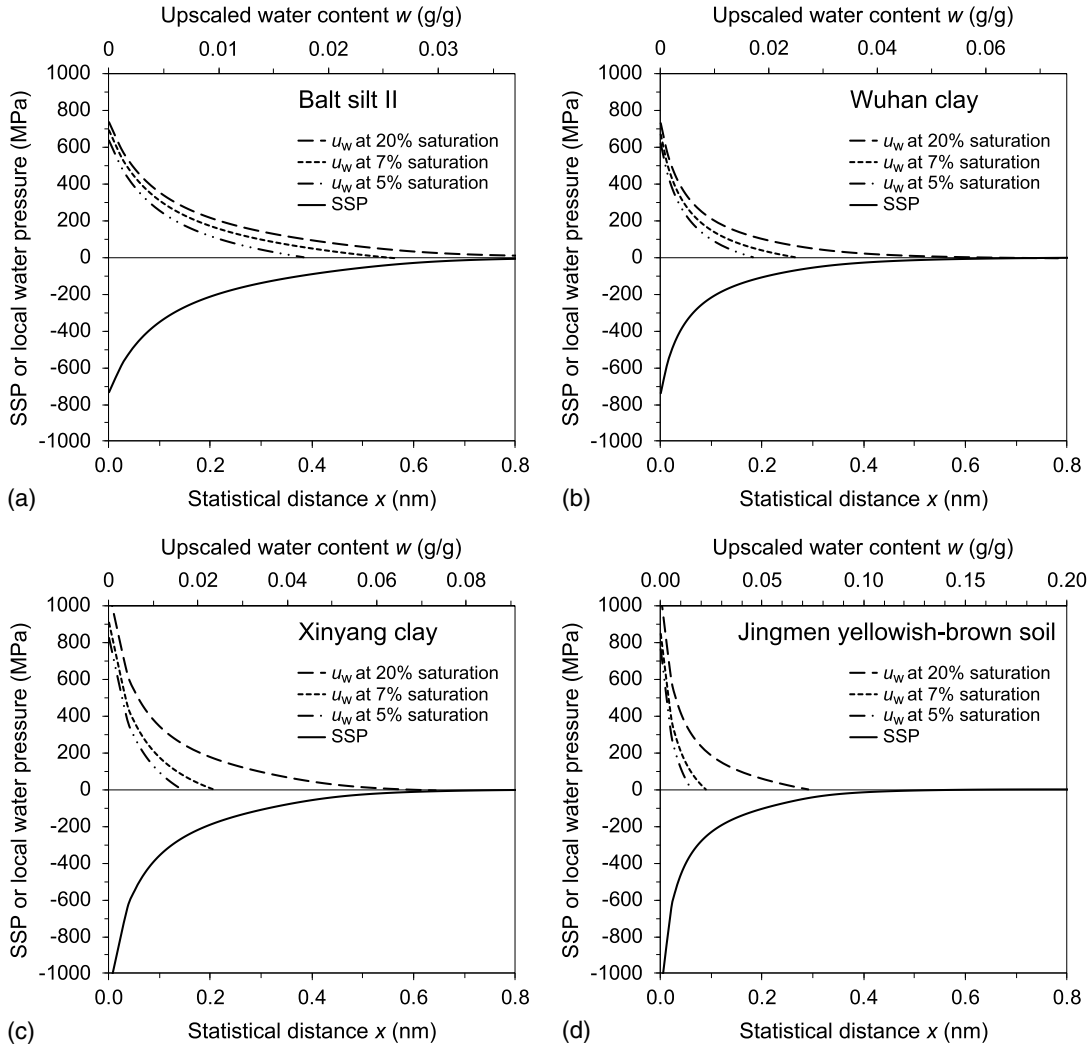

Fig. 10. Soil sorptive potential curves of natural soils and the corresponding local pore water pressure profiles: (a) Balt silt II; (b) Wuhan clay; (c) Xinyang clay; and (d) Jingmen yellowish-brown soil.

The dependence of pore water pressure profile on water content is demonstrated in Fig. 10 by using the four soils in Group 2 at three different water contents (i.e., saturations of 5%, 7%, and 20%). The results illustrate that the distribution of local pore water pressure strongly depends on the soil water content. For a given water content, the predicted pore water pressure starts from a significant positive (compressive) value near the soil particle surface and rapidly decreases farther away. This spatial variation monotonically intensifies with the increasing water content until a soil reaches its saturated water content. In such case matric potential reaches the maximum (0 MPa) and the pore water pressure profile becomes most developed as the exact image of the SSP curve [Eq. (2)]. The highest local pore water pressures (i.e., opposite of the lowest SSP) for the four Group 2 soils are 732, 737, 1,089, and 1,104 MPa (Fig. 10), increasing with the adsorption strengthening.

It can be observed that the same saturation state of soil can associate with different SWR processes, depending on the soil type. For Balt silt II [Fig. 10(a)], the water content at 5% saturation is 0.019 g/g, which corresponds to a water film thickness of 0.38 nm. The pore water pressure determined at the air–water interface is −0.885 MPa below the ambient air pressure (0.101 MPa), indicating that a curved air–water interface has emerged and SWR is in the transitional process of adsorbed film regime. In contrast, 5% saturation for Jingmen yellowish-brown soil also corresponds to a similar water content of 0.018 g/g, but a much thinner water film (0.06 nm) than the Balt silt II formed [Fig. 10(d)]. Water pressure predicted at the air–water interface is identical to the ambient air pressure of 0.101 MPa, demonstrating the tightly adsorbed regime of SWR with flat air–water interface. Given the understanding that water molecules are accumulated around the exchangeable cations on the external surface at the dry end of SWRC, this much smaller water film thickness of 0.06 nm should be interpreted as the normalization of water content to the entire soil surface area.

It can also be observed in Fig. 10 that the water pressure at the air–water interface does not necessarily change with water content monotonically. Instead, it can either increase or decrease as the water content increases, fundamentally dictated by the soil's SSP curve. For instance, Balt silt II has interfacial water pressures of −0.89, −4.63, and −0.21 MPa at saturations of 5%, 7%, and 20%, respectively. When the matric potential is low (e.g., 5% saturation), SSP predominantly controls the SWR over capillarity. The positive part of pore water pressure produced by SSP is large enough to cancel most of the negative pressure produced by capillarity in small pores. As the water content increases continuously, both SSP and capillarity decay but the former is at a faster rate, resulting in a

local minimum (i.e., most negative) of interfacial pore water pressure at 7% among the three saturation conditions.

The local pore water pressure (i.e., intermolecular pressure) is one of the fundamental state variables defining the thermodynamic state of soil water. The pressure profiles determined from the proposed framework illustrate that the local pore water pressure depends not only on the relative spatial location to the soil surface, but also on the soil water content. Both conditions govern the water phase transition in soil such as supercooling, cavitation, and condensation.

Fundamental and Practical Implications

Due to the existence of SSP in soil, the local pore water pressure is always compressive and high (typically up to 800 MPa) near the soil particle surface or within interlamellar layers of clay, no matter whether a soil is in saturated or unsaturated state, or whether the soil is silt or clay. This spatially varying pore water pressure controls many macroscopic soil properties and engineering behaviors such as soil water density (Martin 1962; Zhang and Lu 2018), small-strain shear modulus (Dong and Lu 2016), elastic modulus (Lu 2018), thermal conductivity (Lu and Dong 2015), and soil water freezing curve (Zhang and Lu 2021). The proposed framework for determination of SSP and SWD functions from SWI will open a new experimental pathway to better understand these soil properties.

SSP can be considered as a useful tool to investigate why and how soil swells in the presence of water. Swelling potential is an index commonly used for expansive soil classification in practice (e.g., Holtz and Gibbs 1956; Seed et al. 1962; Chen 1988; McKeen 1992), although it is defined differently. These practically useful swelling potential indexes are empirical and qualitative. Swelling potential is mostly dictated by soil's adsorption, including both the formation of the electrical double layer on the external soil particle surface and the cation hydration and van der Waals forces within the expansive clay mineral interlayers (e.g., Keren and Shainberg 1975; Sposito and Prost 1982; Lu and Khorshidi 2015). All the preceding physicochemical mechanisms have been theorized as part of the SSP concept. In addition to the well-recognized osmotic component of SSP (i.e., osmotic swelling), the proposed framework enables the prediction of local water pressure of a soil at any given water content, which could be used as the physical basis to better define swelling potential in future research.

Summary and Conclusions

Soil sorptive potential has been recognized as an inherent soil matrix property that fundamentally dictates the soil properties and soil water retention behaviors in the adsorptive-prevailing regime. The SSP is a nonlinear decay function of statistical distance x with the minimum (most negative) magnitude near the soil particle surface, which can be linked to soil matric potential through soil water retention curve and soil water density function. Considering the vapor sorption isotherm is an available tool for accurately characterizing the SWRC at relatively low matric potential range, a coupled conceptual and experimental framework was proposed to determine the SSP by taking full advantage of the soil water isotherm in the full relative humidity range.

The proposed framework for SSP determination consists of three sequential steps: SWI fitting, SWD calculation, and SSP determination. A closed-form SWI model was first used to fit the experimental SWI data such that the adsorptive water content was explicitly separated from the capillary water content; then the SWD curve can be calculated as the water content–based weighted average of adsorptive and capillary components. The SSP is equivalent to the adsorptive portion of matric potential at the air–water interface, whose average distance to the soil particle surface can be scaled down from water content with the aid of SWD. Consequently, the whole SSP curve was completely quantified based on the SWRC derived from the fitted SWI.

The SWD curves calculated for both nonswelling and highly swelling clays were compared with experimental SWD measurements reported in the literature. The predicted SWD curves can enclose most of the physical measurements over a wide range of water content, validating the proposed framework for determining SWD. The derived SSP curves of pure Georgia kaolinite and Wyoming montmorillonite match well with SSP fitted through the theoretical equations. Also, the pertinent governing parameters calibrated from this fitting process, including the Hamaker constant and decay length of structural parameter, show excellent agreement with the values of the corresponding soils documented in the literature. Both of these comparisons provide further confirmation of the validity of the proposed framework to determine SSP for different soil types.

SSP is the origin causing spatially varying soil properties such as pore water pressure, soil water density, and water phase transition in soil. The proposed framework is readily implementable for determination of SSP in soils via a stand-alone vapor sorption experiment, enabling direct applications of the SSP concept and better understanding of soil physical behavior in geotechnical and geoenvironmental engineering problems.

Data Availability Statement

All data, models, and code generated or used during the study appear in the published article.

Acknowledgments

This research is supported by the US National Science Foundation (NSF CMMI-1902045).

References

Bahramian, Y., A. Bahramian, and A. Javadi. 2017. "Confined fluids in clay interlayers: A simple method for density and abnormal pore pressure interpretation." *Colloids Surf., A* 521 (May): 260–271. https://doi.org/10.1016/j.colsurfa.2016.08.021.

Bittelli, M., and M. Flury. 2009. "Errors in water retention curves determined with pressure plates." *Soil Sci. Soc. Am. J.* 73 (5): 1453–1460. https://doi.org/10.2136/sssaj2008.0082.

Campbell, G. S., and S. Shiozawa. 1992. "Prediction of hydraulic properties of soils using particle-size distribution and bulk density data." In *Proc., Int. Workshop on Indirect Methods for Estimating the Hydraulic Properties of Unsaturated Soils*, edited by M. T. Van Genuchten, F. J. Leij, and L. J. Lund, 317–328. Berkeley, CA: University of California Press.

Chen, F. H. 1988. *Foundations on expansive soils*. New York: Elsevier.

Cho, C. H., J. Urquidi, S. Singh, S. C. Park, and G. W. Robinson. 2002. "Pressure effect on the density of water." *J. Phys. Chem. A* 106 (33): 7557–7561. https://doi.org/10.1021/jp0136260.

Croney, D., and J. D. Coleman. 1961. "Pore pressure and suction in soil." In *Conference on pore pressure and suction in soils*, 31–37. London: Butterworths.

De Wit, C. T., and P. L. Arens. 1950. "Moisture content and density of some clay minerals and some remarks on the hydration pattern of clay." In *Proc., 4th Int. Congress of Soil Science Transactions*, 59–62. Groningen, Netherlands: Hoitsema Brothers.

Dong, Y., and N. Lu. 2016. "Correlation between small-strain shear modulus and suction stress in capillary regime under zero total stress conditions." *J. Geotech. Geoenviron. Eng.* 142 (11): 4016056. https://doi.org/10.1061/(ASCE)GT.1943-5606.0001531.

Dong, Y., and N. Lu. 2020. "Measurement of suction stress and soil deformation at high suction range." *Geotech. Test. J.* 44 (2): 308–322. https://doi.org/10.1520/GTJ20190357.

Dong, Y., C. Wei, and N. Lu. 2020. "Identifying soil adsorptive water by soil water density." *J. Geotech. Geoenviron. Eng.* 146 (7): 2820001. https://doi.org/10.1061/(ASCE)GT.1943-5606.0002289.

Edlefsen, N. E., and A. B. C. Anderson. 1943. "Thermodynamics of soil moisture." *Hilgardia* 15 (2): 31–298. https://doi.org/10.3733/hilg.v15n02p031.

Guo, Y., and X. B. Yu. 2017. "Characterizing the surface charge of clay minerals with atomic force microscope (AFM)." *AIMS Mater. Sc.* 4 (3): 582–593. https://doi.org/10.3934/matersci.2017.3.582.

Hayward, A. T. J. 1967. "Compressibility equations for liquids: A comparative study." *Br. J. Appl. Phys.* 18 (7): 965–977. https://doi.org/10.1088/0508-3443/18/7/312.

Holtz, W. G., and H. J. Gibbs. 1956. "Engineering properties of expansive clays." *Trans. Am. Soc. Civ. Eng.* 121 (1): 641–663. https://doi.org/10.1061/TACEAT.0007325.

Iwata, S. 1972. "Thermodynamics of soil water: 1. The energy concept of soil water." *Soil Sci.* 113 (3): 162–166. https://doi.org/10.1097/00010694-197203000-00003.

Keren, R., and I. Shainberg. 1975. "Water vapor isotherms and heat of immersion of Na/Ca-montmorillonite systems—I: Homoionic clay." *Clays Clay Miner.* 23 (3): 193–200. https://doi.org/10.1346/CCMN.1975.0230305.

Khorshidi, M., and N. Lu. 2017. "Determination of cation exchange capacity from soil water retention curve." *J. Eng. Mech.* 143 (6): 4017023. https://doi.org/10.1061/(ASCE)EM.1943-7889.0001220.

Likos, W. J., and N. Lu. 2003. "Automated humidity system for measuring total suction characteristics of clay." *Geotech. Test. J.* 26 (2): 179–190. https://doi.org/10.1520/GTJ11321J.

Likos, W. J., N. Lu, and W. Wenzel. 2011. "Performance of a dynamic dew point method for moisture isotherms of clays." *Geotech. Test. J.* 34 (4): 373–382. https://doi.org/10.1520/GTJ102901.

Lu, N. 2016. "Generalized soil water retention equation for adsorption and capillarity." *J. Geotech. Geoenviron. Eng.* 142 (10): 4016051. https://doi.org/10.1061/(ASCE)GT.1943-5606.0001524.

Lu, N. 2018. "Generalized elastic modulus equation for unsaturated soil." In *Proc., 2nd Pan-American Conf. on Unsaturated Soils*, 32–48. Reston, VA: ASCE.

Lu, N. 2020. "Unsaturated soil mechanics: Fundamental challenges, breakthroughs, and opportunities." *J. Geotech. Geoenviron. Eng.* 146 (5): 2520001. https://doi.org/10.1061/(ASCE)GT.1943-5606.0002233.

Lu, N., M. T. Anderson, W. J. Likos, and G. W. Mustoe. 2008. "A discrete element model for kaolinite aggregate formation during sedimentation." *Int. J. Numer. Anal. Methods Geomech.* 32 (8): 965–980. https://doi.org/10.1002/nag.656.

Lu, N., and Y. Dong. 2015. "Closed-form equation for thermal conductivity of unsaturated soils at room temperature." *J. Geotech. Geoenviron. Eng.* 141 (6): 4015016. https://doi.org/10.1061/(ASCE)GT.1943-5606.0001295.

Lu, N., and M. Khorshidi. 2015. "Mechanisms for soil-water retention and hysteresis at high suction range." *J. Geotech. Geoenviron. Eng.* 141 (8): 4015032. https://doi.org/10.1061/(ASCE)GT.1943-5606.0001325.

Lu, N., and W. J. Likos. 2004. *Unsaturated soil mechanics*. New York: Wiley.

Lu, N., and C. Zhang. 2019. "Soil sorptive potential: Concept, theory, and verification." *J. Geotech. Geoenviron. Eng.* 145 (4): 4019006. https://doi.org/10.1061/(ASCE)GT.1943-5606.0002025.

Luo, S., W. J. Likos, and N. Lu. 2021. "Cavitation of water in soil." *J. Geotech. Geoenviron. Eng.* 147 (8): 4021079. https://doi.org/10.1061/(ASCE)GT.1943-5606.0002598.

Luo, S., and N. Lu. 2021. "Validating the generality of a closed-form equation for soil water isotherm." *J. Geotech. Geoenviron. Eng.* 147 (12): 4021138. https://doi.org/10.1061/(ASCE)GT.1943-5606.0002681.

Martin, R. T. 1962. "Adsorbed water on clay: A review." In *Proc., 9th National Conf. on Clays and Clay Minerals*, 28–70. Oxford: Pergamon.

McKeen, R. G. 1992. "A model for predicting expansive soil behavior." In *Proc., 7th Int. Conf. on Expansive Soils*, 1–6. Dallas, TX: Texas Tech Univ.

Nitao, J. J., and J. Bear. 1996. "Potentials and their role in transport in porous media." *Water Resour. Res.* 32 (2): 225–250. https://doi.org/10.1029/95WR02715.

Novich, B. E., and T. A. Ring. 1984. "Colloid stability of clays using photon correlation spectroscopy." *Clays Clay Miner.* 32 (5): 400–406. https://doi.org/10.1346/CCMN.1984.0320508.

Philip, J. R. 1977. "Unitary approach to capillary condensation and adsorption." *J Chem Phys* 66 (11): 5069–5075. https://doi.org/10.1063/1.433814.

Revil, A., and N. Lu. 2013. "Unified water isotherms for clayey porous materials." *Water Resour. Res.* 49 (9): 5685–5699. https://doi.org/10.1002/wrcr.20426.

Richards, B. G. 1965. "Measurement of the free energy of soil moisture by the psychrometric technique using thermistors." In *Moisture equilibria and moisture changes in soils beneath covered areas*, 39–46. Sydney, Australia: Butterworths.

Seed, H. B., R. J. Woodward Jr., and R. Lundgren. 1962. "Prediction of swelling potential for compacted clays." *J. Soil Mech. Found. Div.* 88 (3): 53–87. https://doi.org/10.1061/JSFEAQ.0000431.

Smith, M. W., and A. R. Tice. 1988. *Measurement of the unfrozen water content of soils: Comparison of NMR and TDR methods*. Hanover, NH: Cold Regions Research and Engineering Laboratory.

Solone, R., M. Bittelli, F. Tomei, and F. Morari. 2012. "Errors in water retention curves determined with pressure plates: Effects on the soil water balance." *J. Hydrol.* 470–471 (Nov): 65–74. https://doi.org/10.1016/j.jhydrol.2012.08.017.

Sposito, G., and R. Prost. 1982. "Structure of water adsorbed on smectites." *Chem. Rev.* 82 (6): 553–573. https://doi.org/10.1021/cr00052a001.

Tuller, M., and D. Or. 2005. "Water films and scaling of soil characteristic curves at low water contents." *Water Resour. Res.* 41 (9): W09403. https://doi.org/10.1029/2005WR004142.

Watanabe, K., and T. Wake. 2009. "Measurement of unfrozen water content and relative permittivity of frozen unsaturated soil using NMR and TDR." *Cold Reg. Sci. Technol.* 59 (1): 34–41. https://doi.org/10.1016/j.coldregions.2009.05.011.

Zhang, C., Y. Dong, and Z. Liu. 2017. "Lowest matric potential in quartz: Metadynamics evidence." *Geophys. Res. Lett.* 44 (4): 1706–1713. https://doi.org/10.1002/2016GL071928.

Zhang, C., and N. Lu. 2018. "What is the range of soil water density? Critical reviews with a unified model." *Rev. Geophys.* 56 (3): 532–562. https://doi.org/10.1029/2018RG000597.

Zhang, C., and N. Lu. 2019. "Unitary definition of matric suction." *J. Geotech. Geoenviron. Eng.* 145 (2): 2818004. https://doi.org/10.1061/(ASCE)GT.1943-5606.0002004.

Zhang, C., and N. Lu. 2020. "Soil sorptive potential: Its determination and predicting soil water density." *J. Geotech. Geoenviron. Eng.* 146 (1): 4019118. https://doi.org/10.1061/(ASCE)GT.1943-5606.0002188.

Zhang, C., and N. Lu. 2021. "Soil sorptive potential–based paradigm for soil freezing curves." *J. Geotech. Geoenviron. Eng.* 147 (9): 4021086. https://doi.org/10.1061/(ASCE)GT.1943-5606.0002597.

Zhou, B., and N. Lu. 2021. "Assessments of water sorption methods to determine soil's specific surface area." *J. Geotech. Geoenviron. Eng.* 147 (8): 4021066. https://doi.org/10.1061/(ASCE)GT.1943-5606.0002579.